Biochemical and Biophysical Research Communications 371 (2008) 5–9

Contents lists available at ScienceDirect

Biochemical and Biophysical Research Communications

journal homepage: www.elsevier.com/locate/ybbrc

A circular loop of the 16-residue repeating unit in ice nucleation protein

Yasuhiro Kumaki [a], Keiichi Kawano [b], Kunio Hikichi [c], Takeshi Matsumoto [c], Norio Matsushima [c,*]

[a] High-Resolution NMR Laboratory, Graduate School of Science, Hokkaido University, Sapporo 060-0810, Japan
[b] Division of Biological Sciences, Graduate School of Science, Hokkaido University, Sapporo 060-0810, Japan
[c] School of Health Sciences, Sapporo Medical University, Sapporo 060-8556, Japan

ARTICLE INFO

Article history:
Received 7 March 2008
Available online 24 March 2008

Keywords:
INP
Tandem repeat
Circular loop
Aromatic ring interaction

ABSTRACT

Ice nucleation protein (INP) from Gram-negative bacteria promotes the freezing of supercooled water. The central domain of INPs with 1034–1567 residues consists of 58–81 tandem repeats with the 16-residue consensus sequence of AxxxSxLTAGYGSTxT. This highly repetitive domain can also be represented by tandem repeats of 8-residues or 48-residues. In order to elucidate the structure of the tandem repeats, NMR measurements were made for three synthetic peptides including QTARKGSDLTTGYGSTS corresponding to a section of the repetitive domains in *Xanthomonas campestris* INP. One remarkable observation is a long-range NOE between the side chains of Tyr(*i*) and Ala(*i*-10) in the 17-residue peptide. Medium-range NOEs between the side chains of Tyr(*i*) and Leu(*i*-4), Thr(*i*-3) or Thr(*i*-2) were also observed. These side chain-side chain interactions can be ascribed to CH/π interaction. Structure calculation reveals that the 17-residue peptide forms a circular loop incorporating the 11-residue segment ARKGSDLTTGY.

Heterogeneous ice nucleators promote the freezing of supercooled water and raise the freezing point of the water [1–5]. A heterogeneous ice nucleator aligns water molecules on its surface in an ice-like pattern; this acts as a template for crystallization of ice [6]. Bacterial ice nucleation protein (INP) is one of the most active nucleators. INP is located at the outer membrane of Gram-negative epiphytic bacteria [1]. INP can catalyze ice formation at temperatures as high as 271 K [3,4]. This function of INP is opposite to that of antifreeze proteins which inhibit ice crystal growth [3,7].

The amino acid sequences of 10 INPs from eight species are available [8–19]. Bacterial INPs are 1034–1567 residues long and contain three unique domains; the non-repetitive N-terminal domain, the highly repetitive central domain (HRC domain), and the non-repetitive C-terminal domain (Fig. 1A). The largest, central domain consists of about 20 tandem repeats having a 48-residue consensus sequence (Fig. 1B). This 48-residue sequence can be subdivided into three 16-residue repeats and further divided into six 8-residue repeats (Fig. 1C) [2]. Such nested periodicities of repetition are observed in all INPs.

Some models of HRC domain have been proposed. The proposed models include helical structures with 8-, 16-, 24- or 48-residues per turn [6,13,20–22]. In contrast, there is less experimental research on the structure of the HRC domain. Three structural studies have been performed by NMR and circular dichroism using synthetic or recombinant peptides with 24-, 46- or 96-residues which correspond to a section of the HRC domain in *Pseudomonas syringae* INP [22–24]. For only the shortest 24-residue peptide—AGVDSSLIAGYGSTQTSGSD SALT—was the assignment of ^{1}H NMR resonances completed [23]. A hairpin structure at the segment LIAGY was proposed on the basis of the nuclear Overhauser effect (NOE).

The purpose of this study is to elucidate experimentally the structure of the HRC domain. The NMR experiment was performed using relatively short peptides of 17- and 24-residues corresponding to the HRC domain of INPs. Three peptides used here are basic, differing from the acidic peptides in the previous studies [22,23]. The present work indicates that 17-residue peptide—QTARKGSDLTTGYGSTS—forms a circular loop.

Material and methods

Samples. We designed three peptides.

- **Pep1**: Ac-Q^{1}T^{2}A^{3}R^{4}K^{5}G^{6}S^{7}D^{8}L^{9}T^{10}T^{11}G^{12}Y^{13}G^{14}S^{15}T^{16}S^{17}-NH$_2$.
- **Pep2**: Ac-D^{1}S^{2}S^{3}L^{4}T^{5}A^{6}G^{7}Y^{8}G^{9}S^{10}T^{11}Q^{12}T^{13}A^{14}R^{15}K^{16}G^{17}-NH$_2$.
- **Pep3**: H-S^{1}G^{2}L^{3}R^{4}S^{5}V^{6}L^{7}T^{8}A^{9}G^{10}Y^{11}G^{12}S^{13}S^{14}L^{15}I^{16}S^{17}G^{18}R^{19}R^{20} S^{21}S^{22}L^{23}T^{24}-OH.

Pep1 corresponds to the amino acid residues 440–456 and 680–696 in *Xanthomonas campestri* XC_0519/XCC0507 [18,19]. **Pep2** corresponds to 429–445 in XC_0519/XCC0507 [18,19] and 455–471, 647–663, 695–711, 743–759, 791–807, 887–903, and 935–951 in inaX [17]. **Pep3** corresponds to 873–896 and 1098–1121 in iceE [13,14], 826–849 in inaU [16], and 1114–1137 in inaA [15]. These peptides were purchased from SIGMA Genosys Japan K.K. (Ishikari, Japan). All peptides

* Corresponding author. Fax: +81 11 613 7134.
E-mail address: matusima@sapmed.ac.jp (N. Matsushima).

0006-291X/$ - see front matter © 2008 Elsevier Inc. All rights reserved.
doi:10.1016/j.bbrc.2008.03.069

Fig. 1. Structural organization of ice nucleation protein (INP)—XCC0507 and XC_0519—from *X. campestris pv. campestris*. The amino acid sequences of XCC0507 and XC_0519 are completely identical and are 1333-residues long. (A) Three characteristic domains of INP. The three domains consist of non-repetitive N-terminal domain ("N-domain"), highly repetitive central domain ("HRC domain"), and non-repetitive C-terminal domain ("C-domain"). The HRC domain is 1090-residues long, while the N- and C-terminal domains are 177- and 68-residues long, respectively. (B) The amino acid sequence of XCC0507/XC_0519. The HRC domain indicates sequence alignment based on 48-residue repeat that occurs twenty times. Red and green corresponds to **Pep1** and blue and green corresponds to **Pep2**, showing that green is the overlapping sequence of **Pep1** and **Pep2**. (C) The schematic view of three nested repeats for the HRC domain (in B). The consensus sequences of 8-, 16- and 48-residue repeats are presented. Bold uppercase letters indicates more than 80% occurrence of a given residue in a certain position and normal uppercase letters indicate 70–80% occurrence. Bold lowercase letters with parentheses indicate 50–70% occurrence, and normal lowercase letters indicate 25–50% occurrence in one of residues in parentheses and then more than 80% in all the residues. "x" indicates any amino acid. (For interpretation of color mentioned in this figure the reader is referred to the web version of the article.)

were chemically synthesized using solid-phase Fmoc chemistry on an Applied Biosystems Japan Ltd. Pioneer peptide synthesizer. Synthetic peptides were purified by reverse-phase HPLC using a TSKgel ODS-80Ts column (Tosoh Coop. Japan). The NMR samples of **Pep1** and **Pep2** contain 3 mM of the peptides dissolved in 90%/10% H_2O/D_2O (pH 4.4) with DSS as an internal reference (0.0 ppm), while that of **Pep3** contains 6 mM of the peptide dissolved in 90%/10% H_2O/D_2O 50 mM acetate buffer (pH 4.0) with TSP as an internal reference (0.0 ppm). All of these three NMR samples contain 0.5 mM NaN_3.

NMR measurements. All NMR spectra were measured on JEOL ALPHA 500 spectrometers. Sequence specific assignments of proton resonances were obtained by TOCSY [25] (mixing time = 100 ms), ROESY [26] (mixing time = 150 ms), and DQF-COSY [27] experiments at 278 K (Supplementary Table 1). The 2D NMR spectra were measured in the phase-sensitive mode using TPPI-State for quadrature detection in f_1. Water signal was suppressed by presaturation or WATERGATE method in TOCSY and NOESY [28], and by coherence selection with pulsed field gradients in DQF-COSY experiments. Temperature coefficients of chemical shifts of amide proton resonances ($-\Delta\delta\Delta T$) were estimated from TOCSY spectra (4096 × 512) at 278 and 293 K or 303 K. The $^3J_{HNH\alpha}$ coupling constants were derived from the absorptive and dispersive components of f_2 active splittings of DQF-COSY spectra at 278 K [29].

Structure calculation. For **Pep1**, 56 unambiguously assigned NOE correlations were used to calculate structure (Supplementary Table 2). The NOE correlations were derived from ROESY spectra in 278 K with a mixing time of 150 ms. The NOE cross-peaks were classified as strong (<2.8 Å), medium (<3.3 Å), weak (<5.0 Å), and very weak (<6.0 Å). The pseudo-atom corrections were applied to the protons that were not stereo-specifically assigned [30]. For the NOE correlations involving methyl groups, an additional 0.5 Å was added to the upper distance limit to account for the higher apparent intensity of methyl resonances [31]. The φ dihedral angle of T^2 in **Pep1** was restricted to the range of −160 to −80°, since the $^3J_{HNH\alpha}$ was larger than 8.0 Hz.

The structure calculations were performed with standard protocols for hybrid distance geometry-dynamic simulated annealing method (dg_sa.inp) as implemented in the program CNS 1.1 [32]. In order to perform the calculation of the solution structure for this peptide that has the N-terminal acetyl and C-terminal amide capping groups, the standard topology, parameter and linkage files were modified. Initially, two hundred substructures were calculated by distance geometry. These structures were then subjected to restrained molecular dynamics in Cartesian coordinate space. The molecular dynamics were run for 3 ps at a temperature of 2000 K with a time step of 3 *f*s, followed by cooling to 0 K in 25 K steps with 60 *f*s at each temperature. During the cooling stage, the force constant on the van der Waals repulsion term was varied from 0.003 to 4 kcal mol^{-1} $Å^{-4}$. Finally, restrained energy minimization with the conjugate gradient method was performed. This stage consisted of 2000 steps. The force constants on the dihedral angle restraints were 200 kcal mol^{-1} rad^{-2} during molecular dynamics and 400 kcal mol^{-1} rad^{-2} during energy minimization. The force constant on NOE restraints was 50 kcal mol^{-1} $Å^{-2}$ throughout all calculations. Fifteen structures with lower energies out of 200 calculated structures were selected as final structures. Analysis and evaluation of calculated structures were performed by MOLMOL [33] and PROCHECK [34].

Results

NMR resonance assignments

The identification of individual amino acid residues was completed unambiguously by TOCSY and DQF-COSY experiments for **Pep1**. H^α of Gly and H^β of Ser were distinguished by DQF-COSY. Two sets of spin networks in TOCSY spectrum were observed for D^8. The spin network with low-field shifted D^8 NH resonance is reasonably assigned to be the major species because of their larger intensity of the cross-peaks. The sequential assignments were completed unambiguously by ROESY experiment which observes intraresidue NOEs and sequential NOEs between $H^\alpha(i)$ and NH($i+1$). Only the sequential NOE $H^\alpha(i)$–NH($i+1$) was not observed between T^{16} and S^{17}, while NOE $H^\beta(i)$–NH($i+1$) was observed. Similarly, for **Pep2** and **Pep3**, the identification of individual amino acid residues and their sequential assignments were completed unambiguously. The NMR data are given in Supplementary Table 1 and in the BioMagRes data bank (Accession Code 15639, 15640, and 15641).

Medium- and long-range NOE

For all of the three peptides, medium- and long-range NOE were observed between tyrosine aromatic ring and methyl protons of sequentially non-neighboring residues. For **Pep1**, $Y^{13}H^\varepsilon$ show

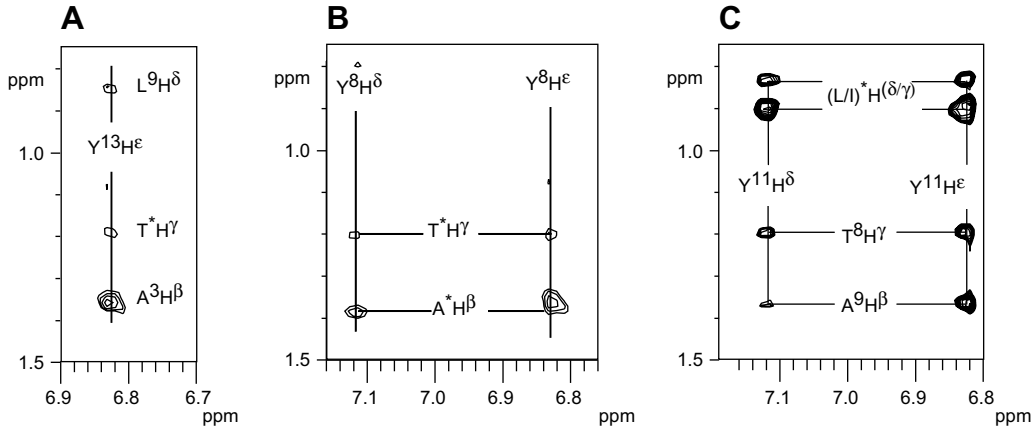

Fig. 2. The expansion of the ROESY spectra showing the cross-peaks between the methyl protons and aromatic protons. (A) **Pep1** (Ac-$Q^1T^2A^3R^4K^5G^6S^7D^8L^9T^{10}T^{11}$-$G^{12}Y^{13}G^{14}S^{15}T^{16}S^{17}$-$NH_2$); (B) **Pep2** (Ac-$D^1S^2S^3L^4T^5A^6G^7Y^8G^9S^{10}T^{11}Q^{12}T^{13}A^{14}R^{15}K^{16}G^{17}$-$NH_2$); (C) **Pep3** (H-$S^1G^2L^3R^4S^5V^6L^7T^8A^9G^{10}Y^{11}G^{12}S^{13}S^{14}L^{15}I^{16}S^{17}G^{18}R^{19}R^{20}S^{21}S^{22}L^{23}T^{24}$-OH). In A, T^* indicates T^2, T^{10}, T^{11}, and/or T^{16}. In B, A^* indicates A^6 and/or A^{14}. In C, $(L/I)^*H^{(\delta/\gamma)}$ indicates L^7H^δ, $L^{15}H^\delta$, and/or $I^{16}H^\gamma$ for the resonance with 0.84 ppm, and plus L^3H^δ for the resonance at 0.90 ppm in f_1 dimension.

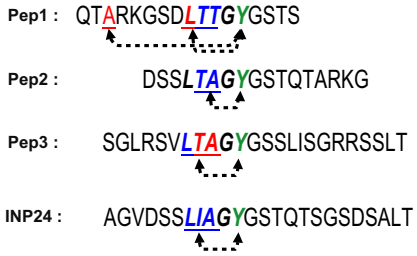

Fig. 3. Summary of medium- or long-range NOE connectivities associated with tyrosine residues. Red letters indicate the residues which are determined unambiguously to be the NOE connected partners of tyrosine residues (green). Blue letters indicate the residues which are not identified unambiguously but assumed to be the most plausible on the basis of their amino acid sequence. For **Pep1**, T^{10} as well as T^{11} is sequentially near to Y^{13}, therefore, these two Thr are shown in blue. The residues within pentapeptide segment L(T/I)(A/T)GY are indicated in bold italic. The NOE connectivities for INP24 were described by Tsuda et al. [23]. (For interpretation of color mentioned in this figure the reader is referred to the web version of the article.)

NOE connectivities with A^3H^β, L^9H^δ and T^*H^γ where T^* indicates T^{10} and/or T^{11} (Fig. 2A). For **Pep2**, Y^8H^δ and Y^8H^ε show NOE connectivities with A^*H^β and T^5H^γ, where A^* indicates A^6 and/or A^{14} (Fig. 2B). For **Pep3**, $Y^{11}H^\delta$ and $Y^{11}H^\varepsilon$ show NOE connectivities with T^8H^γ, A^9H^β, and $(L/I)^*H^{(\delta/\gamma)}$, where $(L/I)^*H^{(\delta/\gamma)}$ indicates L^7H^δ, $L^{15}H^\delta$, and/or $I^{16}H^\gamma$ for the resonance with 0.84 ppm, and plus L^3H^δ for the resonance at 0.90 ppm in f_1 dimension (Fig. 2C). These NOE connectivities for each peptide are summarized in Fig. 3.

Calculated structure

The structure calculation was performed for **Pep1**, as noted. The superimposed backbones of these 15 structures are shown in Fig. 4A. Most of all φ, ψ dihedral angles (93.8%) lie in the allowed regions of Ramachandran map (Supplementary Table 2). The resulting structure gives a circular loop. The pairwise RMSD for the overall backbones is 3.57 Å, while the central part, $A^3R^4K^5G^6S^7D^8L^9T^{10}T^{11}G^{12}Y^{13}$ has smaller RMSD (2.16 Å) (Fig. 4B and Supplementary Table 2). The side chains of A^3, L^9, and Y^{13} are located at the inside of the circular loop (Fig. 4B). This circular loop comprises a turn-like structure at the segment $L^9T^{10}T^{11}G^{12}Y^{13}$. For 8 of the 15 structures the distance between the C^α atoms of L^9 and G^{12} is less than 7 Å, which gives the criterion for identification of β-turn [35].

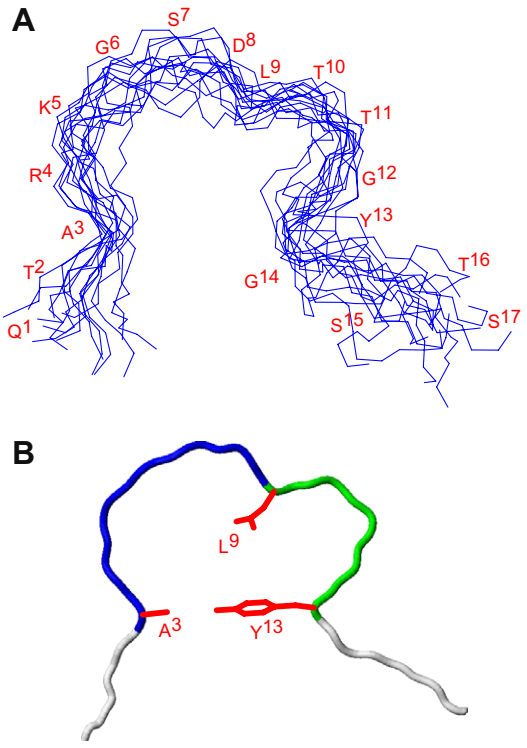

Fig. 4. Calculated structure of **Pep1** (Ac-$Q^1T^2A^3R^4K^5G^6S^7D^8L^9T^{10}T^{11}$-$G^{12}Y^{13}G^{14}S^{15}T^{16}S^{17}$-$NH_2$). (A) Superimposed fifteen backbone structures; (B) mean structure. In B, Backbone chain is represented by the ribbon. Green ribbon shows the pentapetide segment $L^9T^{10}T^{11}G^{12}Y^{13}$ forming a turn-like structure within the circular loop. The other portion of the circular, $A^3R^4K^5G^6S^7D^8$, is shown by blue ribbon. The both terminal region, Q^1T^2 and $G^{14}S^{15}T^{16}S^{17}$, are shown in white ribbon. Red indicates the side chains of A^3, L^9, and Y^{13}. (For interpretation of color mentioned in this figure the reader is referred to the web version of the article.)

The far-UV CD spectra for **Pep1** did not indicate the presence of regular secondary structures (data not shown), suggesting that this circular loop is flexible.

Discussion

The HRC domain in INP is characterized by three nested repeats having the 48-residue high-fidelity, the 16-residue medium-fidel-

ity, and 8-residue low-fidelity, as noted. As shown in Fig. 1C, the consensus sequence of the 16-residue repeats in the HRC domain of *X. campestris* XC_0519/XCC0507 may be represented by **A**xxx**S**x**L**(**t**i)**AGYGST**x**T** in which, for comparison, its "phasing" (that is, what residue corresponds to the beginning of a repeating unit) was changed.

*Turn-like structure of the segment **L(ti)AGY***

Pep1 includes LTTGY, while both **Pep2** and **Pep3** include LTAGY. The segment LTTGY in **Pep1** adopts a β-turn-like structure, which is mainly due to NOE between Y(i) and L($i-4$), T($i-3$) or T($i-2$). In **Pep2** and **Pep3** NOE were observed between Y(i) and L($i-4$), and moreover between Y(i) and T($i-3$) or A($i-2$) with ambiguity. Thus, as well as the segment LTTGY in **Pep1**, the segment LTAGY in both peptides adopts presumably a turn-like structure. Similarly, the NMR experiment has been performed for the peptide of AGVDSSLIAGYGSTQTSGSDSALT (**INP24**), corresponding to the section within the HRC domain of *P. syringae* INP. The analysis suggested that the segment LIAGYG adopted a hairpin loop, which mainly results from NOE between Y(i) and L($i-4$), I($i-3$) or A($i-2$) [23]. It can be concluded that L(T/I)(A/T)GY in the HRC domain adopt a turn-like structure similar to β-turn.

The segments of LTTGY, LTAGY or LIAGY correspond to **L**(**t**i)**AGY** in the consensus sequence of the 16-residue repeats (Fig. 1C). All of the conservative pentapeptide segments forms probably the turn-like structure in the HRC domain.

*Circular loop of the segment **AxxxSxL(ti)AGY***

The most significant result is that the segment $A^3R^4K^5G^6S^7D^8L^9T^{10}T^{11}G^{12}Y^{13}$ in **Pep1** forms a circular loop structure which is mainly due to the interaction between A^3 and Y^{13}; A($i-10$) and Y(i). However, such an interaction was not observed in **Pep2** and **Pep3** from the following reasons. **Pep2** lacks an amino acid corresponding to the A($i-10$). In **Pep3**, S^1 corresponding to the A($i-10$) is located on the N-terminus. Thus S^1 appears to be very mobile. INP24 include the segment $A^1G^2V^3D^4S^5S^6L^7I^8A^9G^{10}Y^{11}$, corresponding to $A^3R^4K^5G^6S^7D^8L^9T^{10}T^{11}G^{12}Y^{13}$ in **Pep1.** Because H^β chemical shifts of A^1 and A^9 were consistent [23], NOE connectivities observed are identified not only between A^9 and Y^{11} and but also between $A^1$and Y^{11}. Thus, a circular loop seen in **Pep1** may be formed in the segment $A^1G^2V^3D^4S^5S^6L^7I^8A^9G^{10}Y^{11}$.

The above observations indicate that the interactions between tyrosine aromatic ring and methyl groups of the Ala, Leu, and/or Thr are crucial for the formation of the circular loop in **Pep1**. Aromatic ring such as Tyr, Phe, and Trp frequently participates in weak interactions involving aromatic-aromatic interaction [36–39], cation–π interaction [40,41] and amino–aromatic interactions [42]. In addition, there is CH/π interaction [43]. CH/π interaction occurs between hydrogens attached to carbon (–CH) as a donor and π electron of aromatic ring as an acceptor [43]; this contributes significantly to the stability of protein structure [44]. Consequently, it can be concluded that the CH/π interaction contributes to the stability of the circular loop structure.

A plausible β-helix structure of HRC domain in INP

It is instructive to compare the 16-residue repeats in INP with **Pep1**. Three residues A^3, L^9, and Y^{13}, in **Pep1** ($Q^1T^2A^3R^4K^5G^6S^7D^8L^9T^{10}T^{11}G^{12}Y^{13}G^{14}S^{15}T^{16}S^{17}$) are important for the formation of the circular loop, because their three side chains interact with each other and are located in the inside of the loop structure (Fig. 4B). The consensus sequence of the 16-residue repeats in the HRC domain may be represented by **A**xxx**S**x**L**(**t**i)**AGYGST**x**T** (Fig. 1C). Thus, A^3, L^9, and Y^{13} in **Pep1** correspond to Ala at position 1, Leu at position 7 and Tyr at position 11 in the 16-residue consensus sequence, respectively.

Spruce budworm antifreeze protein (AFP) contains six tandem repeats of STxTxxxazxxxxaxx where "T" is Thr, "a" is Ile or Tyr, "S" is Ser or Thr, "x" is any amino acid and "z" is deletion. It is significant to compare this 15-/16-residue repeat with the 16-residue repeats, **ST**x**TA**xxx**S**x**L**(**t**i)**AGYG**, in the HRC domain (Fig. 1C). These two consensus sequences are the same in the four N-terminal sequences, STxT. This AFP adopts β-helix that is composed of the repetition of the helical loop unit, each of which includes one or three β-strands of the STxT motif [45]. These patterns of amino acid sequence and the present NMR results suggest that the HRC domain may adopt a β-helix consisting of 16-residues per turn [22].

Implications of the circular loop for ice-nucleation activity

The STxT motifs in AFP form a flat face of parallel β-sheets [46,47]. On this face, Thr's form two parallel arrays that match the ice lattice and are crucial for the antifreeze activity [48]. The HRC domain can interact with ice through the STxT face. The AFP β-helix structure is stabilized by the disulfide bridges. In contrast, the circular loop observed is formed by weak interactions such as the CH/π interaction. The INP β-helix is presumably less stable than the AFP β-helix. This difference may influence the ice nucleation activity of INP and the antifreeze activity of AFP.

Acknowledgments

We thank Dr. Robert H. Kretsinger of University of Virginia for his valuable suggestion and comments. This work was supported by a Grant-in-Aid for Scientific Research from the Ministry of Education, Science, Sports and Culture of Japan (to Y.K.).

Appendix A. Supplementary data

Supplementary data associated with this article can be found, in the online version, at doi:10.1016/j.bbrc.2008.03.069.

References

[1] P. Wolber, G. Warren, Bacterial ice-nucleation proteins, Trends Biochem. Sci. 14 (1989) 179–182.
[2] G. Warren, P. Wolber, Molecular aspects of microbial ice nucleation, Mol. Microbiol. 5 (1991) 239–243.
[3] C.L. Hew, D.S. Yang, Protein interaction with ice, Eur. J. Biochem. 203 (1992) 33–42.
[4] D. Gurian-Sherman, S.E. Lindow, Bacterial ice nucleation: significance and molecular basis, FASEB J. 7 (1993) 1338–1343.
[5] H. Kawahara, The structures and functions of ice crystal-controlling proteins from bacteria, J. Biosci. Bioeng. 94 (2002) 492–496.
[6] A.V. Kajava, S.E. Lindow, A model of the three-dimensional structure of ice nucleation proteins, J. Mol. Biol. 232 (1993) 709–717.
[7] S.P. Graether, B.D. Sykes, Cold survival in freeze-intolerant insects: the structure and function of β-helical antifreeze proteins, Eur. J. Biochem. 271 (2004) 3285–3296.
[8] R.L. Green, G.J. Warren, Physical and functional repetition in a bacterial ice nucleation gene, Nature 317 (1985) 645–648.
[9] W.G. Miller, J.H. Leveau, S.E. Lindow, Improved gfp and inaZ broad-host-range promoter-probe vectors, Mol. Plant Microbe Interact. 13 (2000) 1243–1250.
[10] D. Schmid, D. Pridmore, G. Capitani, R. Battistutta, J.-R. Neeser, A. Jann, Molecular organisation of the ice nucleation protein InaV from *Pseudomonas syringae*, FEBS Lett. 414 (1997) 590–594.
[11] H.C. Jung, J.G. Pan Submitted (JUL-1997) to the EMBL/GenBank/DDBJ databases.
[12] G.J. Warren, L. Corotto, P. Wolber, Conserved repeats in diverged ice nucleation structural genes from two species of *Pseudomonas*, Nucleic Acids Res. 14 (1986) 8047–8060.
[13] G.J. Warren, L. Corotto, The consensus sequence of ice nucleation proteins from *Erwinia herbicola*, *Pseudomonas fluorescens* and *Pseudomonas syringae*, Gene 85 (1989) 239–242.
[14] D. Gurian-Sherman, S.E. Lindow, N.J. Panopoulos, Isolation and characterization of hydroxylamine-induced mutations in the *Erwinia*

herbicola ice nucleation gene that selectively reduce warm temperature ice nucleation activity, Mol. Microbiol. 9 (1993) 383–391.
[15] K. Abe, S. Watabe, Y. Emori, M. Watanabe, S. Arai, An ice nucleation active gene of *Erwinia ananas*: sequence similarity to those of *Pseudomonas* species and regions required for ice nucleation activity, FEBS Lett. 258 (1989) 297–300.
[16] Y. Michigami, S. Watabe, K. Abe, H. Obata, S. Arai, Cloning and sequencing of an ice nucleation active gene of *Erwinia uredovora*, Biosci. Biotechnol. Biochem. 58 (1994) 762–764.
[17] J.L. Zhao, C.S. Orser, Conserved repetition in the ice nucleation gene inaX from *Xanthomonas campestris pv. Translucens*, Mol. Gen. Genet. 223 (1990) 163–166.
[18] W. Qian, Y. Jia, S.X. Ren, Y.Q. He, J.X. Feng, L.F. Lu, Q. Sun, G. Ying, D.J. Tang, et al., Comparative and functional genomic analyses of the pathogenicity of phytopathogen *Xanthomonas campestris pv. Campestris*, Genome Res. 15 (2005) 757–767.
[19] A.C.R. da Silva, J.A. Ferro, F.C. Reinach, C.S. Farah, L.R. Furlan, R.B. Quaggio, C.B. Monteiro-Vitorello, et al., Comparison of the genomes of two *Xanthomonas* pathogens with differing host specificities, Nature 417 (2002) 459–463.
[20] G. Warren, P. Wolber, Heterogeneous ice nucleation by bacteria, Cryo. Lett. 8 (1987) 204–215.
[21] H. Mizuno, Prediction of the conformation of ice-nucleation protein by conformational energy calculation, Proteins Struct. Funct. Genet. 5 (1989) 47–65.
[22] S.P. Graether, Z.C. Jia, Modeling *Pseudomonas syringae* ice-nucleation protein as a β-helical protein, Biophys. J. 80 (2001) 1169–1173.
[23] S. Tsuda, A. Ito, N. Matsushima, A hairpin-loop conformation in tandem repeat sequence of the ice nucleation protein revealed by NMR spectroscopy, FEBS Lett. 409 (1997) 227–231.
[24] Y. Kobashigawa, Y. Nishimiya, K. Miura, S. Ohgiya, A. Miura, S. Tsuda, A part of ice nucleation protein exhibits the ice-binding ability, FEBS Lett. 579 (2005) 1493–1497.
[25] L. Braunschweiler, R.R. Ernst, Coherence transfer by isotropic mixing: application to proton correlation spectroscopy, J. Magn. Reson. 53 (1983) 521–528.
[26] D.G. Davis, A. Bax, Practical aspects of two-dimensional transverse NOE spectroscopy, J. Magn. Reson. 63 (1985) 207–213.
[27] U. Piantini, O.W. Sørensen, R.R. Ernst, Multiple quantum filters for elucidating NMR coupling networks, J. Am. Chem. Soc. 104 (1982) 6800–6801.
[28] M. Piotto, V. Saudek, V. Sklenár, Gradient-tailored excitation for single-quantum NMR spectroscopy of aqueous solutions, J. Biomol. NMR 2 (1992) 661–665.
[29] Y. Kim, J.H. Prestegard, Measurement of vicinal couplings from cross peaks in COSY spectra, J. Magn. Reson. 84 (1989) 9–13.
[30] K. Wüthrich, M. Billeter, W. Braun, Pseudo-structures for the 20 common amino acids for use in studies of protein conformations by measurements in intramolecular proton–proton distance constraints with nuclear magnetic resonance, J. Mol. Biol. 169 (1983) 949–961.
[31] G.M. Clore, A.M. Gronenborn, M. Nilges, C.A. Ryan, Three-dimensional structure of potato carboxypeptidase inhibitor in solution: a study using nuclear magnetic resonance, distance geometry, and restrained molecular dynamics, Biochemistry 26 (1987) 8012–8023.
[32] A.T. Brünger, P.D. Adams, G.M. Clore, W.L. Delano, P. Gros, R.W. Grosse-Kunstleve, J.S. Jiang, et al., Crystallography & NMR system: a new software suite for macromolecular structure determination, Acta Crystallogr. D Biol. Crystallogr. 54 (1998) 905–921.
[33] R. Koladi, M. Billeter, K. Wüthrich, MOLMOL: a program for display and analysis of macromolecular structures, J. Mol. Graph. 14 (1996) 51–55.
[34] R.A. Laskowski, M.W. MacArthur, D. Moss, J.K. Thornton, PROCHECK: a program to check the stereochemical quality of protein structures, J. Appl. Cryst. 26 (1993) 283–291.
[35] C.M. Wilmot, J.M. Thornton, Analysis and prediction of the different types of β-turn in proteins, J. Mol. Biol. 203 (1988) 221–232.
[36] S.K. Burley, G.A. Petsko, Aromatic–aromatic interaction: a mechanism of protein structure stabilization, Science 229 (1985) 23–28.
[37] U. Samanta, D. Pal, P. Chakrabarti, Packing of aromatic rings against tryptophan residues in proteins, Acta Crystallogr. D Biol. Crystallogr. 55 (1999) 1421–1427.
[38] R. Chelli, F.L. Gervasio, P. Procacci, V. Schettino, Stacking and T-shape competition in aromatic-aromatic amino acid interactions, J. Am. Chem. Soc. 124 (2002) 6133–6143.
[39] C.A. Hunter, J. Singh, J.M. Thornton, π–π interactions: the geometry and energetics of phenylalanine-phenylalanine interactions in proteins, J. Mol. Biol. 218 (1991) 837–846.
[40] N.S. Scrutton, A.R. Raine, Cation–π bonding and amino–aromatic interactions in the biomolecular recognition of substituted ammonium ligands, Biochem. J. 319 (1996) 1–8.
[41] J.P. Gallivan, D.A. Dougherty, Cation–π interactions in structural biology, Proc. Natl. Acad. Sci. USA 96 (1999) 9459–9464.
[42] S.K. Burley, G.A. Petsko, Amino–aromatic interactions in proteins, FEBS Lett. 203 (1986) 139–143.
[43] Y. Umezawa, M. Nishio, CH/π interactions in the crystal structure of TATA-box binding protein/DNA complexes, Bioorg. Med. Chem. 6 (1998) 2507–2515.
[44] M. Brandl, M.S. Weiss, A. Jabs, J. Sühnel, R. Hilgenfeld, C–H...π -interactions in proteins, J. Mol. Biol. 307 (2001) 357–377.
[45] E.K. Leinala, P.L. Davies, D. Doucet, M.G. Tyshenko, V.K. Walker, Z. Jia, A β-helical antifreeze protein isoform with increased activity. Structural and functional insights, J. Biol. Chem. 277 (2002) 33349–33352.
[46] E.K. Leinala, P.L. Davies, Z. Jia, Crystal structure of β-helical antifreeze protein. Points to a general ice binding model, Structure 10 (2002) 619–627.
[47] Y.C. Liou, A. Tocilj, P.L. Davies, Z.C. Jia, Mimicry of ice structure by surface hydroxyls and water of a β-helix antifreeze protein, Nature 406 (2000) 322–324.
[48] S.P. Graether, M.J. Kuiper, S.M. Gagné, V.K. Walker, Z.C. Jia, B.D. Sykes, P.L. Davies, β-Helix structure and ice-binding properties of a hyperactive antifreeze protein from an insect, Nature 406 (2000) 325–328.